Article ID: 1003－6326(2003)05－1149－06

Numerical solution to T- $\varphi_S C_L$ coupling in binary dendrite solidification with any solid-back diffusion effects①

XU Da-ming(徐达鸣), GUO Jing-jie(郭景杰), FU Heng-zhi(傅恒志),
SU Yan-qing(苏彦庆), LI Qing-chun(李庆春)
(School of Materials Science and Engineering, Harbin Institute of Technology, Harbin 150001, China)

Abstract: A previous numerical solution method to the strong nonlinear T- $\varphi_S C_L$ coupling for a Scheil-type binary solidification process was extended and modified for single-phase dendrite solidifications of any nominal alloy composition (in a composition range of single-phase or eutectic solidification) and with any solid-back diffusion extents. Numerical sample computations were performed on Al-Cu system with different nominal compositions from almost pure Al to nearly eutectic and with different solid diffusion coefficients, which are factitiously enlarged or decreased in eight orders of magnitude. The calculation results exhibit the feasibility, capability and efficiency of the proposed numerical scheme in modeling an arbitrary binary dendrite solidification problem.

Key words: alloy solidification; coupled transport phenomena; solid-back diffusion; numerical modeling
CLC number: TF 771.2; TG 244 **Document code:** A

1 INTRODUCTION

Most alloy materials in engineering applications solidify in a temperature range and in dendritic manners. Such complicated liquid-to-solid phase-change processes are usually controlled simultaneously by heat, mass and momentum transfers, and determined by the alloy's nonlinear properties of solidification thermodynamics/kinetics. It has been shown that a continuum or mixture average model has the mathematical succinctness and relative numerical-solution efficiency in modeling the dendritic solidification-transport-phenomena (STP)[1-7]. However, in addition to the complexities of the dendritic STP-based modeling, there exist several nonlinear and strong couplings among each transport process. One of the important couplings is the correlation among the solidifying temperature, volume fraction of the solid phases and the liquid composition, i.e. the T- $\varphi_S C_L$ coupling. In a previous work[8], a simultaneously numerical method was proposed to solve this strong nonlinear T- $\varphi_S C_L$ coupling in a binary dendrite solidification problem, but only for the solidification cases with negligible solid-back diffusion (SBD) within the solidifying phases, i.e. for a Scheil-type solidification[9].

However, in a realistic dendrite solidification process, the SBD effects may vary continuously from zero to infinite depending on the alloy properties and solidification conditions (primarily, the solid-diffusion-coefficient, D_S, and the solidification rate, R_f). In a recent micro/macro-scale modeling for solute-mass-transport in dendrite solidification[10], the continuum model previously proposed by the present authors[8] was extended to a general binary solidification case with any incomplete SBD and any dendritic morphology. This adds some mathematical difficulties to the numerical model computations, especially for the T- $\varphi_S C_L$ coupling solution. Therefore, the aim of this work is to extend and modify the numerical solution procedures previously developed for the T- $\varphi_S C_L$ coupling of Scheil-type solidification in order to accommodate the any incomplete SBD issue in dendrite solidification processes. Numerical solution samples will be performed on Al-Cu binary system and shaped castings with different nominal compositions and solid-diffusion-coefficients to demonstrate the feasibility and capabilities of the extended numerical method.

2 NUMERICAL MODEL SOLUTION

In the present work, a general binary solidification case with any SBD effects and dendrite morphologies, in which the solidifying dendrites are assumed to be macroscopically static, is considered. Such a five-independent-variable STP problem can be described by the continuum model (a single-domain model[6]) that was newly modified and extended in Refs. [10, 11]. From this mathematical model it can be seen that, the jointly varying solidification temperature, T, volume fraction of solid phase, φ_S and the liquid concentration, C_L, compose a strong and nonlinear T- $\varphi_S C_L$ coupling in determining the alloy so-

① **Foundation item:** Project(G2000067202-2) supported by the National Key Fundamental Research and Development Program of China
Received date: 2002－10－15; **Accepted date:** 2003－03－14
Correspondence: XU Da-ming, Professor; Tel: +86-451-86418624; E-mail: damingxu@hit.edu.cn

lidification processes. In order to solve the proposed solidification model as accurate as possible, this T- φ_S C_L correlation has to be numerically treated at the same given time level of t^{i+1}. Ref. [8] has illustrated the simultaneous T- $\varphi_S C_L$ changing behavior in a Scheil-type solidification process, and proposed the relevant numerical solution methodology. However, when any SBD effects are incorporated into the solidification model, as expressed by Eqns. (1) ~ (4) of Ref. [11], the T- $\varphi_S C_L$ coupling behavior will be different depending on the SBD extents, even under the same solidification conditions for the same alloys. This is schematically illustrated in Fig. 1 for a binary alloy of nominal composition less than the alloy's maximum solid limit, i.e. $C_0 < C_{SM}$.

Under the assumptions of sufficient interdendritic liquid mixing and thermodynamic equilibrium held at the S/L interface, the interdendritic liquid concentration, $C_L (= C_L^*)$, and the interface solid concentration, C_S^*, always follow the liquidus and solidus of the alloy system, respectively, during solidification no matter how strong the SBD is. Whereas, the locally averaged composition within the solidified phases, $C_{SA} (= \overline{C}_S)$, behaves differently depending on the SBD extents. For a Scheil-type solidification mode, C_{SA} follows the curve labeled with "SBD= 0" in Fig. 1(a), and a fractional eutectic phase will always form no matter how low the nominal composition of the alloy, C_0, is[9], see the "SBD= 0"-labeled $\varphi_S T$ curve in Fig. 1(b). Furthermore, for this zero SBD case, the solidification always terminates at the eutectic temperature, T_E. For another extreme case of a lever-rule type solidification, the composition C_{SA} strictly follows the alloy's solidus curve and terminates at $T_{Sol}(C_0)$, and no eutectic phase will form because $C_0 < C_{SM}$. While for a more practical solidification case with any incomplete SBD extents (i.e. a case of $0 < \Phi < 1$ by the present modeling), the C_{SA}- T and $\varphi_S T$ curves vary between that of the two extreme solidification cases, see the curves labeled with "0< SBD< ∞" in Fig. 1(a) and (b). In the latter case, the freezing termination temperature, T_{SB}, and if or how much a fractional eutectic phase will form, all depend on the SBD extents occurring in the dendrite solidification process. The solidification behaviors for a binary alloy of nominal composition: $C_{SM} \leqslant C_0 \leqslant C_E$ are similar to that shown in Fig. 1, except a volume fraction of eutectic phase will always form and the eutectic quantity will depend on the SBD effects. In the following, the previous numerical solution methodology for a Scheil-type solidification[8] will be extended and modified in order to accommodate the arbitrary SBD effects on the strong nonlinear T- $\varphi_S C_L$ coupling that can be changed from zero continuously to infinite.

For computation convenience, a 2-D explicit finite difference scheme is adopted to discretize the present solidification model, i.e. Eqns. (2) ~ (4) and (10) ~ (14) of Ref. [11]. This scheme can easily separate the T- $\varphi_S C_L$ coupling with that for liquid momentum transfer numerically. In this arti-

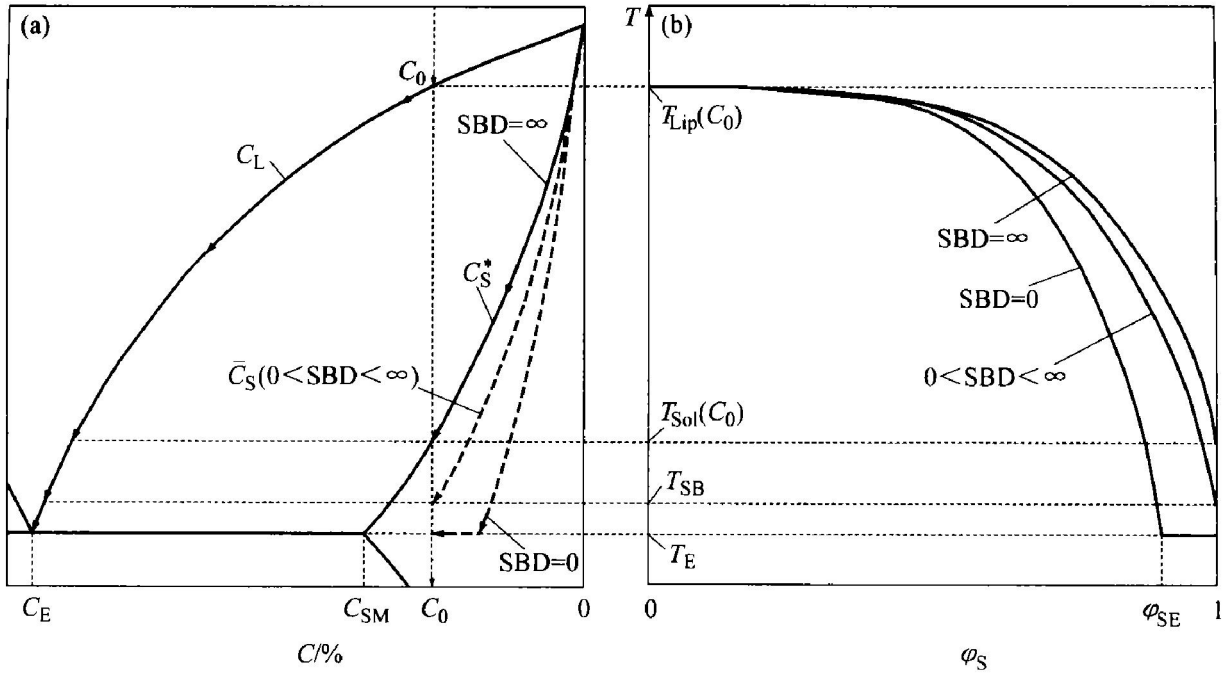

Fig. 1 Solidification behaviors of binary alloy of nominal composition $C_0 < C_{SM}$ and with different solid-back diffusion (SBD) extents (Local thermodynamic equilibrium holds at micro-scale S/L interface)

(a) —A portion of binary alloy phase diagram with solidification paths of C_L, C_S^* and $\overline{C}_S$ for different SBD; (b) —Corresponding curves of solid fraction versus liquidus temperature

cle, the emphasis is focused on the numerical solution to the nonlinear correlation of T-$\varphi_S C_L$ with arbitrary SBD effects. The numerical solution scheme for the momentum transport of liquid flow and the strong P-V coupling is basically same as that described in Ref. [12].

The same 2-D meshing pattern and coordinate system for a casting/ingot domain as illustrated in Ref. [8] (Fig. 2) are used for the present numerical approaches. The 2-D continuum model-based numerical formula for the heat energy transport for control volume $[j, k]$ can be derived as

$$T^{i+1}_{j,k} = \{T_{F0}\cdot T^{i}_{j,k} - \Delta t^{i+1}\{c^{i}_{pLj,k}\cdot[(T_{VY1}-T_{VY2})/\Delta y_j + (T_{VZ1}-T_{VZ2})/\Delta z_k] - [(T_{DY1}-T_{DY2})/\Delta y_j + (T_{DZ1}-T_{DZ2})/\Delta z_k]\}\}/T_{F1} \quad (1)$$

where the terms of T_{VY1}, T_{VY2}, T_{VZ1}, T_{VZ2}, T_{DY1}, T_{DY2}, T_{DZ1}, T_{DZ2}, T_{F0} and T_{F1} take the same expression forms as those listed in Ref. [8]. In Eqn. (1), the temperature- and composition-dependent alloy properties for different phases, such as the specific heats, c_{PL}/ c_{PS}, and the thermal conductivity, k_m, etc, have been taken into account.

Based on the author's unified Φ-parameter modeling, i.e. Eqns. (11) and (2)-(4) of Ref. [11], a 2-D discretized equation for the species mass transport of $[j, k]$-volume can be written as

$$C^{i+1}_{Lj,k} = \{C_{F0}\cdot C^{i}_{Lj,k} - \Delta t^{i+1}\{[(C_{VY1}-C_{VY2}) + (C_{DY1}-C_{DY2})]/\Delta y_j - [(C_{VZ1}-C_{VZ2}) + (C_{DZ1}-C_{DZ2})]/\Delta z_k\}\}/C_{F1} \quad (2)$$

where

$$C_{VY1} = C^{i}_{Lj,k}\cdot\max(RFV\,Y^{i}_{j+1/2,k}, 0) + C^{i}_{Lj+1,k}\cdot\max(RFV\,Y^{i}_{j+1/2,k}, 0)$$

$$C_{VY2} = C^{i}_{Lj-1,k}\cdot\max(RFV\,Y^{i}_{j-1/2,k}, 0) + C^{i}_{Lj,k}\cdot\max(RFV\,Y^{i}_{j-1/2,k}, 0)$$

$$C_{VZ1} = C^{i}_{Lj,k}\cdot\max(RFV\,Z^{i}_{j,k-1/2}, 0) + C^{i}_{Lj,k-1}\cdot\max(RFV\,Y^{i}_{j,k-1/2}, 0)$$

$$C_{VZ2} = C^{i}_{Lj,k+1}\cdot\max(RFV\,Z^{i}_{j,k+1/2}, 0) + C^{i}_{Lj,k}\cdot\max(RFV\,Y^{i}_{j,k+1/2}, 0)$$

$$C_{DY1} = \{D^{i}_{Lj+1/2,k}\cdot[(\varphi_L\cdot\rho_L\cdot C_L)^{i}_{j+1,k} - (\varphi_L\cdot\rho_L\cdot C_L)^{i}_{j,k}] + D^{i}_{Sj+1/2,k}\cdot[(\varphi_S\cdot\rho_S\cdot\overline{C_S})^{i}_{j+1,k} - (\varphi_S\cdot\rho_S\cdot\overline{C_S})^{i}_{j,k}]\}/\Delta y_{j+1/2}$$

$$C_{DY2} = \{D^{i}_{Lj-1/2,k}\cdot[(\varphi_L\cdot\rho_L\cdot C_L)^{i}_{j,k} - (\varphi_L\cdot\rho_L\cdot C_L)^{i}_{j-1,k}] + D^{i}_{Sj-1/2,k}\cdot[(\varphi_S\cdot\rho_S\cdot\overline{C_S})^{i}_{j,k} - (\varphi_S\cdot\rho_S\cdot\overline{C_S})^{i}_{j-1,k}]\}/\Delta y_{j-1/2}$$

$$C_{DZ1} = \{D^{i}_{Lj,k-1/2}\cdot[(\varphi_L\cdot\rho_L\cdot C_L)^{i}_{j-1,k} - (\varphi_L\cdot\rho_L\cdot C_L)^{i}_{j,k}] + D^{i}_{Sj,k-1/2}\cdot[(\varphi_S\cdot\rho_S\cdot\overline{C_S})^{i}_{j,k-1} - (\varphi_S\cdot\rho_S\cdot\overline{C_S})^{i}_{j,k}]\}/\Delta z_{k-1/2}$$

$$C_{DZ2} = \{D^{i}_{Lj,k+1/2}\cdot[(\varphi_L\cdot\rho_L\cdot C_L)^{i}_{j,k+1} - (\varphi_L\cdot\rho_L\cdot C_L)^{i}_{j,k}] + D^{i}_{Sj,k+1/2}\cdot[(\varphi_S\cdot\rho_S\cdot\overline{C_S})^{i}_{j,k+1} - (\varphi_S\cdot\rho_S\cdot\overline{C_S})^{i}_{j,k}]\}/\Delta z_{k+1/2}$$

$$C_{F0} = (\varphi_L\cdot\rho_L)^{i}_{j,k} + \Phi^{i}_{j,k}\cdot\varphi^{i}_{Sj,k}\cdot(\rho^{*}_{L}\cdot k)^{i}_{j,k}$$

$$C_{F1} = (\varphi_L\cdot\rho_L)^{i+1}_{j,k} + (\Delta\varphi^{i+1}_{Sj,k} + \Phi^{i}_{j,k}\cdot\varphi^{i}_{Sj,k})\cdot(\rho^{*}_{L}\cdot k)^{i+1}_{j,k}$$

This new formula is suitable for the macroscopic species mass transport in a dendrite solidification process with any SBD extents and dendrite morphologies. Similar to the numerical species-mass-transport equation previously derived for Scheil-type solidification[8], Eqn. (2) again indicates that the interdendritic-liquid concentration, $C^{i+1}_{Lj,k}$, will increase (for a system with partition coefficient $k<1$) with the solidification proceeding, f_s increasing, for any SBD conditions.

As discussed in the previous work[8], the temperature calculated by Eqn. (1), $T^{i+1'}_{j,k}$, only represents the value that corresponds to the heat-energy change caused by the conductive and convective terms in the time interval of $\Delta t^{i+1} = t^{i+1} - t^{i}$. Based on the heat-energy balance principle and the thermodynamic equilibrium solidification assumption, the following numerical formula has been proposed to account for the latent heat term and to calculate the solid fraction increment, $\Delta\varphi^{i+1}_{Sj,k}$, in the Δt^{i+1} time interval:

$$\Delta\varphi^{i+1}_{Sj,k} = [(\varphi_S\cdot\rho_S\cdot c_{pS} + \varphi_L\cdot\rho_L\cdot c_{pL})/(\rho_S\cdot h)]^{i}_{j,k}\cdot(T^{i+1}_{liqj,k} - T^{i+1'}_{j,k}) \quad (3)$$

where $T^{i+1}_{liqj,k} = F(C^{i+1}_{Lj,k})$ is the liquidus temperature of alloy determined by the liquid concentration. This formula is still applicable to the present numerical approaches to the T-$\varphi_S C_L$ coupling with any SBD effects. Again, the superscript "i" or "$i+1$" onto all the alloy properties terms, e.g. $D^{i}_{Sj,k+1/2}$, $(\rho^{*}_{L}\cdot k)^{i+1}_{j,k}$ and $(\rho_S\cdot h)^{i}_{j,k}$ etc, in Eqns. (2) and (3) accounts for the influences of the temperature or/and composition-dependent properties variations. The numerical Eqns. (1) to (3) compose the basic numerical iteration formulas to solve the T-$\varphi_S C_L$ coupling at time t^{i+1} (to determine $T^{i+1}_{j,k}$, $\Delta\varphi^{i+1}_{Sj,k}$ and $C^{i+1}_{Lj,k}$).

However, as illustrated in Fig. 1 for a binary dendrite solidification process, an important possibility exists that a volume fraction of eutectic phase, $1-\varphi_{SE}$, can form at the final solidification stage, depending on the nominal alloy composition, C_0, the SBD extents, solidification rate and dendrite morphologies etc[10]. For some alloy systems, the eutectic composition, C_E, is possibly so high compared to its maximum solid solution composition, C_{SM}, that even very tiny eutectic fraction formed will significantly influence the calculated compositions of the solidified phases, such as for Al-Cu alloy. Therefore, to achieve a reliable numerical solution to the T-$\varphi_S C_L$ coupling, the eutectic phase fraction must be deter-

mined as accurately as possible. The supplemental formulas to treat such issue, so that the solid fraction for eutectic formation for $[j, k]$-volume can be determined by $\varphi_{SEj,k} = \varphi^{i}_{Sj,k} + \Delta\varphi^{i+1}_{S(BE)j,k}$, are given as follows:

$$\Delta\varphi^{i+1}_{S(BE)} = \Delta\varphi^{i+1}_{S(Cal)} \cdot [(T^i - T_E)/(T^i - T^{i+1}_{liq(Cal)})] \quad (4)$$

$$\Delta\varphi^{i+1}_{S(AE)} = \Delta\varphi^{i+1}_{S(Cal)} \cdot [(T_E - T^{i+1}_{liq(Cal)})/(T^i - T^{i+1}_{liq(Cal)})] \cdot [(\rho_{s\alpha} \cdot h_\alpha)/(\rho_{SE} \cdot h_E)]^{i}_{j,k} \quad (5)$$

where $\Delta f^{i+1}_{S(Cal)j,k}$ is the calculated solid-fraction increment within which the eutectic phase starts to form.

3 RESULTS AND DISCUSSION

To demonstrate the feasibility and efficiency of the present numerical solution procedure to the strongly coupled nonlinear dendrite solidification problems with any SBD, numerical computations are performed with Al-Cu solidification samples of different nominal compositions and different solid solute diffusivities. Nine different alloy compositions of Al-0.001%, 0.5%, 2.0%, 4.5%, 8.0%, 14.0%, 20.0%, 28.0% and 32.0% Cu (mass fraction) are chosen, and five different levels of temperature-dependent solid-diffusion coefficients of $10^{-3} \times D_S(T)$, $0.1 \times D_S(T)$, $D_S(T)$, $10 \times D_S(T)$ and $10^5 \times D_S(T)$ are assumed for the present sample computations. The STP-based binary solidification model, i.e. Eqns. (2)~(4) and (10)~(14) of Ref. [11], are fully solved with the numerical formulas of Eqns. (1)~(5), in a iteration procedure[8], and a modified numerical method similar to that previously proposed for the gravity- and solidification-shrinkage-induced liquid flow in dendrite solidification[12].

The above binary alloys with a 2-D blade-like casting shape are assumed to solidify in a directional freezing furnace at a constant withdrawal velocity of 0.15 mm/s. The solidification configuration, casting/shell mold dimensions, meshing pattern and varying alloy properties used are the same as those adopted in Ref. [11]. The computation results shown in the followings are only for a control volume at the bottom of the directionally solidified blade-like castings for the present investigation purposes. This means that the present T-φ_S-C_L solution results are for an open solidification volume[13] and with varying solidification rates in a range of 0.008–0.42 s^{-1} for the whole solidification process according to the recorded modeling computation results[11].

Figs. (2) and (3) show the comparisons of the calculated $C_L - \varphi_S$ and $C_{SA} - \varphi_S$ curves for the Al-4.5% Cu dendrite solidification with different assumed solid-diffusion coefficients. In these figures, the curves labeled with "$D_S(T)$" correspond to the true alloy property case. According to some additional computations with the assumed solid-diffusion coefficients of $10^{-2} \times D_S(T)$ and $10^4 \times D_S(T)$ etc, the present curves calculated with $10^{-3} \times D_S(T)$ and $10^5 \times D_S(T)$ show to be quite close to the Scheil-type and lever-rule-type solidification modes, respectively. It can be seen that under the present solidification case, the alloy volume exhibits a solute-redistribution behavior with an incomplete SBD. At the end of solidification, the concentration of the interdendritic liquid phase reaches the alloy's eutectic composition, C_E = 33.2% Cu, see the "$D_S(T)$"-labeled $C_L - \varphi_S$ curve, and predicts the presence of tiny fraction of eutectic phase.

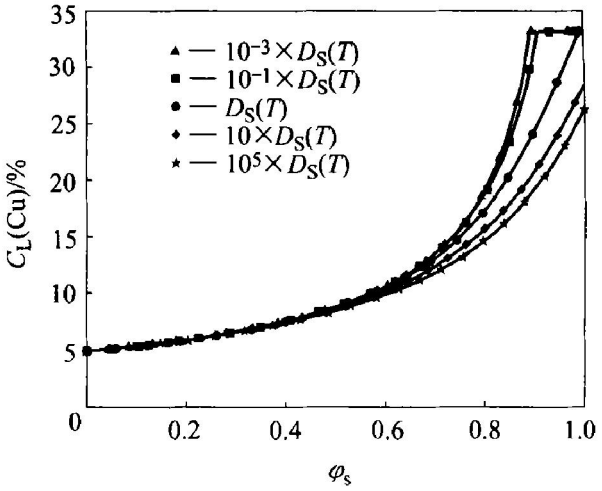

Fig. 2 Comparison of calculated $C_L - \varphi_S$ curves for Al-4.5% Cu dendrite solidification with different assumed solid-diffusion coefficients

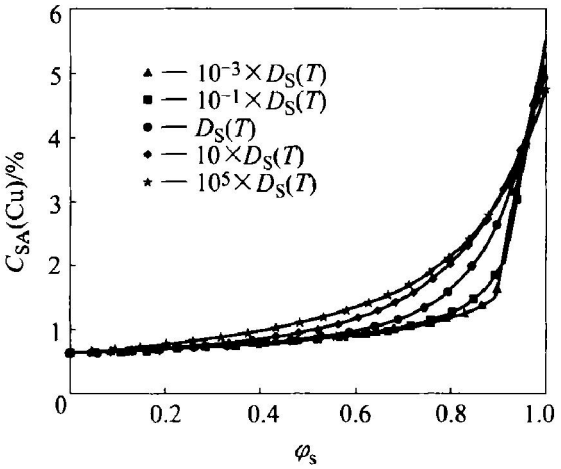

Fig. 3 Comparison of calculated $C_{SA} - \varphi_S$ curves for Al-4.5% Cu dendrite solidification with different assumed solid-diffusion coefficients

From Fig. 2, it also can be seen that when the solid-diffusion coefficient is decreased or increased by an order of magnitude, the corresponding $C_L - \varphi_S$ curve moves towards to those for $10^{-3} \times D_S(T)$ or $10^5 \times D_S(T)$ more closely, respectively. These re-

sults show the significant influences of the solid-diffusion variation on the present solidification and solute-redistribution behaviors. As illustrated in Fig. 1 that, for a close solidification volume, the final averaged solid composition should be always equal to the nominal alloy composition no matter what extent of the SBD occurs. However, from the comparison of the $C_{SA}-\varphi_S$ curves shown in Fig. 3, it can be seen that, with different solid-diffusion coefficients the final averaged solid compositions of these curves are different: the stronger the solid-diffusion, the lower the final C_{SA} value is. This is because that for the present directional solidification case, an inverse macrosegregation, i. e. a positive segregation: $C_{SA} > C_0$, will always form at the bottom of the casting. On the other hand, for an open solidification volume, when the solid diffusion becomes strong, the solutes will diffuse more out of the volume resulting in its final averaged composition C_{SA} lower.

Figs. 4 and 5 show the comparison of the calculated $C_L-\varphi_S$ and $C_S^*-\varphi_S$ curves for Al-Cu dendrite solidification with different nominal compositions but the same solid-diffusion coefficients of $D_S(T)$. All these computational results demon-

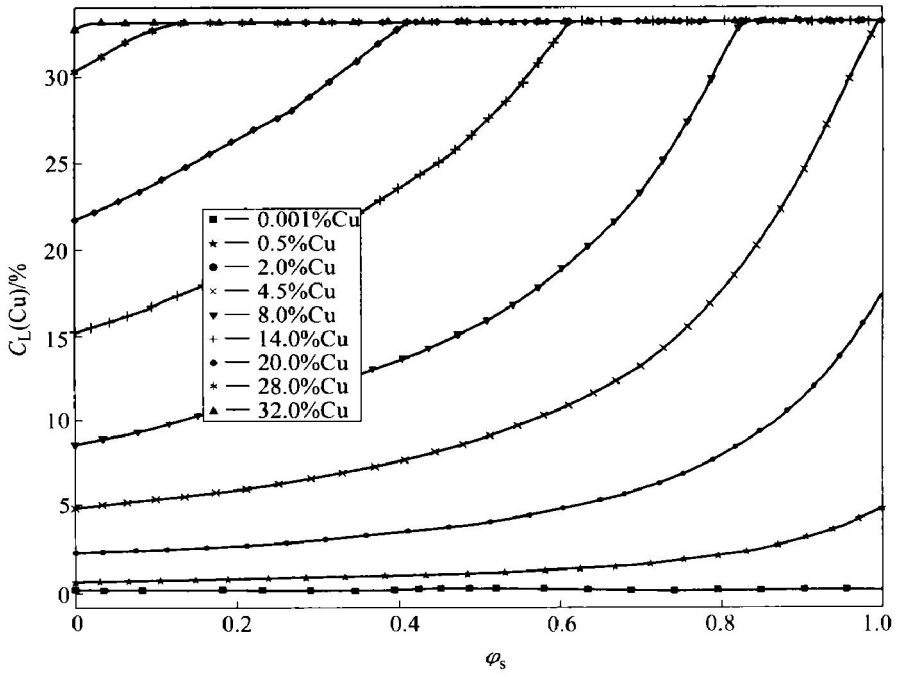

Fig. 4 Comparison of calculated $C_L-\varphi_S$ curves for Al-Cu dendrite solidification with different nominal alloy compositions but same solid-diffusion coefficients $D_S(T)$

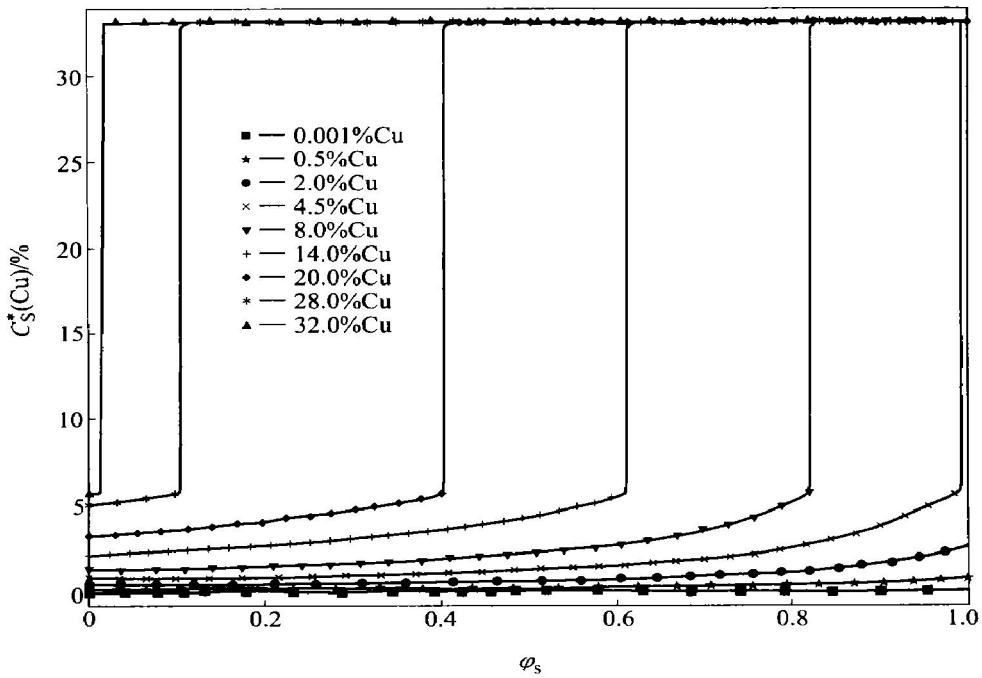

Fig. 5 Comparison of calculated $C_S^*-\varphi_S$ curves for Al-Cu dendrite solidification with different nominal alloy compositions but same solid-diffusion coefficients $D_S(T)$

strate the feasibility and capability of the proposed numerical-solution scheme to the strong nonlinear T-$\varphi_S C_L$ coupling in a binary dendrite solidification process. From the present numerical-solution procedures and the schematic solidification behaviors shown in Fig. 1, it is known that the most computational-effort-consuming portion in treating the T-$\varphi_S C_L$ coupling is the numerical iterations to determine the single-phase solidification behavior, i. e. α(Al) phase for the present case. In all the sample computations for different alloy compositions and with different solid-diffusion coefficients, the iterative times in determining a convergent T-$\varphi_S C_L$ computation at a t^{i+1} time level are mostly among a range of 13 to 25. This indicates that the presently proposed numerical-solution method to the strong nonlinear T-$\varphi_S C_L$ coupling in binary dendrite solidification is efficient.

4 CONCLUSION

In a binary dendrite solidification process, there exist several possible solidification paths depending on the alloy types, the nominal alloy compositions and the SBD effects occurring within the solidifying phases etc. Through the sample computations, the numerical-solution methods presented in this paper show to be feasible and capable to treat all the possible T-$\varphi_S C_L$ coupling cases occurring in a binary dendrite solidification process (single-phase + eutectic) of arbitrary nominal compositions and with any SBD extents. The proposed iteration procedures also show to be efficient in numerically determining a T-$\varphi_S C_L$ correlation balance in the single-phase solidification stage.

REFERENCES

[1] Bennon W D, Incropera F P. A continuum model for momentum, heat and species transport in binary solid-liquid phase change systems —Ⅰ. model formulation and —Ⅱ. application to solidification in a rectangular cavity [J]. Int J Heat Mass Transfer, 1987, 30: 2161-2187.

[2] Voller V R, Brent A D, Prakash C. The modeling of heat, mass and solute transport in solidification systems [J]. Int J Heat Mass Transfer, 1989, 32: 1719-1731.

[3] Poirier D R, Nandapurkar P J, Ganesan S. The energy and solute conservation equation for dendritic solidification [J]. Metall Mater Trans B, 1991, 22: 889-900.

[4] Prescott P J, Incropera F P, Bennon W D. Modeling of dendritic solidification systems: reassessment of the continuum momentum equation [J]. Int J Heat Mass Transfer, 1991, 34: 2351-2359.

[5] Xu D, Li Q, Pehlke R D. Computer simulation of Al-Cu alloy solidification using a continuum model [J]. AFS Trans, 1991, 95: 737-745.

[6] Ni J, Incropera F P. Extension of the continuum model for transport phenomena occuring during metal alloy solidification—Ⅰ. the conservation equations [J]. Int J Heat Mass Transfer, 1995, 38: 1285-1296.

[7] XU Da-ming, LI Qing-chun, AN Ge-ying. Research progress in computer modeling for solidification transport phenomena and macrosegregation in castings and ingots [J]. Foundry, 1997(4): 44-49. (in Chinese)

[8] XU Da-ming, LI Qing-chun. Numerical method for solution of strongly coupled binary alloy solidification problems [J]. Num Heat Transfer, Part A, 1991, 20: 181-201.

[9] Flemings M C. Solidification Processing [M]. New York: McGraw-Hill, 1974. 77-83; 246-252.

[10] XU Da-ming. A unified micro-scale parameter approach to solidification transport phenomena-based macrosegregation modeling for dendritic solidification: part Ⅰ. mixture average based analysis [J]. Metall Mater Trans B, 2001, 32B: 1129-1141.

[11] XU Da-ming. A unified micro-scale parameter approach to solidification transport process-based macrosegregation modeling for dendritic solidification: part Ⅱ. numerical example computations [J]. Metall Mater Trans B, 2002, 33B: 451-463.

[12] XU Da-ming, LI Qing-hun. Gravity- and solidification-shrinkage-induced liquid flow in a horizontally solidified alloy ingot [J]. Num Heat Transfer, Part A, 1991, 20: 203-221.

[13] Rappaz M, Voller V. Modeling of micro-macrosegregation in solidification processes [J]. Metall Mater Trans A, 1990, 21: 749-753.

(Edited by YUAN Sai-qian)